Quantum Transport on Disordered and Noisy Networks: An Interplay of Structural Complexity and Uncertainty

Mattia Walschaers,[1,2] Frank Schlawin,[1] Thomas Wellens,[1] and Andreas Buchleitner[1,3]

[1]Institute of Physics, Albert Ludwigs University of Freiburg, D-79104 Freiburg, Germany; email: mattia.walschaers@physik.uni-freiburg.de, frank.schlawin@physics.ox.ac.uk, thomas.wellens@physik.uni-freiburg.de, a.buchleitner@physik.uni-freiburg.de

[2]Institute for Theoretical Physics, University of Leuven, B-3001 Heverlee, Belgium

[3]Freiburg Institute for Advanced Studies, Albert Ludwigs University of Freiburg, D-79104 Freiburg, Germany

Annu. Rev. Condens. Matter Phys. 2016. 7:223–48

First published online as a Review in Advance on December 21, 2015

The *Annual Review of Condensed Matter Physics* is online at conmatphys.annualreviews.org

This article's doi: 10.1146/annurev-conmatphys-031115-011327

Keywords

quantum transport, quantum control through disorder, many-particle transport, indistinguishability, complex materials

Abstract

We discuss recent research on quantum transport in complex materials, from photosynthetic light-harvesting complexes to photonic circuits. We identify finite, disordered networks as the underlying backbone and as a versatile framework to gain insight into the specific potential of nontrivial quantum dynamical effects to characterize and control transport on complex structures. We discriminate authentic quantum properties from classical aspects of complexity and briefly address the impact of interactions, nonlinearities, and noise. We stress the relevance of what we call the nonasymptotic realm, physical situations in which neither the relevant time- and length-scales, the number of degrees of freedom, or constituents tend to very small or very large values, nor do global symmetries or disorder fully govern the dynamics. Although largely uncharted territory, we argue that novel, intriguing and nontrivial questions for experimental and theoretical work emerge, with the prospect of a unified understanding of complex quantum transport phenomena in diverse physical settings.

1. INTRODUCTION

"Quantum transport" expresses a specific view on the world of quantum phenomena, which originates in condensed matter physics, and, to some extent, physical chemistry: An excitation, an electron or a quasiparticle is to be shipped from input to output of a physical sample to be characterized, possibly by macroscopic quantifiers like its resistivity (1), or to be transferred from some donor to some acceptor molecular unit, typically over mesoscopic scales, to trigger chemical reactions (2, 3). As is immediately apparent when defining input and output states asymptotically, this view is intimately related to scattering theory (with the transmission of a plane wave through a potential barrier as the elementary textbook example). In an alternative perspective, by its very construction, this view defines one of the standard scenarios for nonequilibrium quantum physics. Although historically (and anthropomorphically) set in the spatial degree of freedom, transport can, of course, likewise occur in arbitrary directions of phase space, as well as on the energy axis. Often, however, a change of stage implies a change of research community and jargon: Quantum transport on the energy axis (often the momentum axis in disguise) is witnessed and controlled, e.g., in the physics of light-matter interaction (from strong to feeble electromagnetic fields), and often comes under the alternative label quantum dynamics (4, 5). When decomposable into finite numbers of two-level systems or elementary excitations, at a manageable level of complication, "quantum simulation" as a specific brand of "quantum information" sets out to mimic elementary quantum transport phenomena (6, 7).

The elementary ingredient of quantum transport is incarnated by Young's double slit when taken to the granular level of the self-interference of a single particle: Although this phenomenon is now well understood since Feynman (8), from the underlying dynamics to the emergence of the interference pattern upon integration over single-particle events (9), it gives rise to a panoply of rather dramatic and not-yet-common-sense quantum interference phenomena once the number of interfering amplitudes (and, possibly, particles) is increased. In particular, when we enter the realm of multiple scattering[1] phenomena (again, possibly, but not necessarily, in configuration space), quantum interference effects can prevail, even after averaging over a broad range of randomly chosen physical realizations of the scattering potential,[2] which, on a first glance, appears very counterintuitive when contemplating the fate of Young's double-slit interference pattern upon independent averaging over the slits' positions. Yet the most prominent disorder-induced interference effects, weak (10), strong or Anderson (11), and, in a Hamiltonian setting, dynamical (12) localization bear tangible macroscopic manifestations, from enhanced back-scattering signals [first observed on Saturn's rings (13)] to by now well-defined and well-controlled metal-insulator quantum phase transitions (see the sidebar Weak and Strong Localization) (10, 12, 14–35).

Most importantly, the truly amazing improvement of experimental diagnostic tools and of the experimental control on composite, hybrid quantum systems nowadays allows, arguably for the first time, systematic exploration of the controlled transition from many- to single-particle quantum transport and dynamical phenomena (36–40) on potential landscapes that interpolate, possibly on a hierarchy of scales, between perfect symmetries and disorder (41–46). Beyond the experimental mimicry of well-established theoretical models for extended solids or fields, the truly innovative potential of this rather recent experimental progress lies in charting the largely unknown territory between single-particle quantum dynamics and the thermodynamic limit (39, 47–50), which can be safely predicted to offer plenty of original research questions and surprising answers. Apart

[1] Of a single particle on a complicated potential landscape, and/or of many particles.

[2] Defined, in an actual experiment, e.g., by different, macroscopically identically prepared samples; by slow drifts of the microscopic sample structure or of externally applied fields; by variations of the input state or channels; etc.

WEAK AND STRONG LOCALIZATION

Weak and strong localization are well-defined concepts in condensed matter and mesoscopic transport theory (1, 42). They describe the impact of disorder-induced quantum interference effects on the transmission probability across disordered potential landscapes, which survive the disorder average and can be rather dramatic. Often it is difficult to properly distinguish interference-induced (weak or strong) localization from other mechanisms that impede transport, such as, e.g., (partial) phase space barriers or the somewhat trivial confinement of an eigenstate to one or few local potential minima. Consequently, the terminology tends to be used in a rather fuzzy manner in the literature beyond condensed matter and mesoscopics.

Weak Localization Phenomena

Weak localization consists in a reduction of the diffusion constant, and hence of the transmission probability, due to an enhanced return probability to a given point within the sample. The latter is a consequence of the interference of time-reversed multiple scattering paths and also leads to (enhanced) coherent backscattering of the injected probability flux. Weak localization is often considered to be a precursor of strong localization, in the regime of weak disorder, i.e., for $\ell k \gg 1$, where ℓ is the scattering mean free path and k is the transported particle's wave vector.

Strong Localization Phenomena

Strong or Anderson localization consists in the vanishing of the diffusion constant as a consequence of complete, destructive interference upon transmission. It manifests differently in one, two, and three dimensions and is associated with a quantum phase transition from delocalized to exponentially localized eigenstates on 3D disorder potentials, at $\ell k \simeq 1$. An analogous phenomenon in light-matter interaction at high spectral densities, dubbed "dynamical localization", leads to a suppression of the effective energy transfer from the driving to the matter degree of freedom.

Control of Localization Phenomena

Due to the dramatic impact of localization phenomena on dynamical and spectral features, efforts are being made to exploit or manipulate these effects for the purpose of quantum control, e.g., by tailoring inter-site couplings or by injecting nonlinearities (45, 94).

from offering novel ways to control (quantum) transport properties that ultimately define the efficiency of technological devices (51) [e.g., for light energy conversion, such as light emitting diodes (LEDs) or photovoltaics (PVs)], such endeavors certainly stand to qualitatively improve our understanding of the quantum-to-classical transition (38, 52, 53) as one of the fundamental open issues of quantum theory (and of its interpretation) to date.

A useful and versatile scenario for the study of quantum dynamics in what we here call the nonasymptotic range is a finite network or graph of variable topology, which can mediate transport of one or more particles (54–61). On the one hand, the network's topology allows a flexible transition from order to disorder, and, on the other hand, it offers a broad choice of observables to characterize single- or many-particle transport. The network can be connected to leads (supporting continua of scattering states), to define a bona fide scattering problem (57, 62–64), and/or, locally or globally interfaced with incoherent environments, to incorporate dynamical rather than static disorder—*vulgo* noise (which, on sufficiently long timescales, kills quantum interference; see the sidebar Static Versus Dynamical Noise) (65).

LED: light emitting diode

PV: photovoltaic

STATIC VERSUS DYNAMICAL NOISE

There is an important distinction between disorder and noise: Disorder expresses our lack of knowledge of the precise realization, e.g., of a potential landscape. Disordered systems evolve unitarily, but to obtain descriptions that are robust against variations of the microscopic hardwiring of the generating Hamiltonian, a disorder average has to be performed. This in general leads to dephasing (or inhomogeneous broadening, in spectroscopy jargon), which, however, can in principle be compensated for by spin echo techniques. In contrast, noise stems from uncontrolled temporal fluctuations of the generating Hamiltonian on timescales that are shorter than the timescales of interest and need to be averaged over. This leads to an irreversible loss of information that cannot be recovered, and, in particular, induces decoherence.

The network's topology (beyond, simply, its dimension) can be employed to control the probability of particle encounter and, thus, through the particles' indistinguishability and/or their interaction strength, the structure of the quantum interference terms that control its transport properties (43, 66). Furthermore, a network can be considered the natural backbone of a multitude of physical transport problems, from regular or disordered lattices in one, two, or three dimensions, in configuration, phase, or energy space (54, 67–70), to molecular aggregates in functional materials or biological substrates (58, 71–73), quantum algorithms (74), photonic circuits (75, 76), electromagnetic transmission lines, or multiple scattering media—e.g., cold atomic clouds and Rydberg gases (50, 77, 78)—with slowly (with respect to a single, multiple-scattering event) drifting conformations, and many more. This review exploits this versatility to illustrate the rich phenomenology of quantum interference effects in the nonasymptotic range, between symmetry and disorder, coherence and noise, and distinguishability and discernability. We import concrete examples from recent scientific debates on the role of quantum coherence in biophysical contexts and on controlled many-particle interference in photonic circuits, but we also touch on de facto closely related, though apparently distinct, quantum transport phenomena in other (sub)fields.

2. EXCITATION TRANSPORT ON NETWORKS WITH CONSTRAINED DISORDER

We start out with a paradigmatic single-particle transport problem on finite networks, which has received renewed interest in the interpretation of spectroscopic data of unprecedented quality, on photosynthetic functional units of plants, algae, and photosynthetic bacteria (79, 80), as well as on PV blends useful, e.g., for organic PV devices (81, 82). In the photosynthetic scenario, the energy carried by an incoming photon is transformed into an electronic excitation, forming an exciton (83, 84), which then needs to be transported to what is known as the reaction center, a molecular structure in which the organism uses that incoming energy to create free charges that then feed the reservoir of adenosine triphosphate (ATP) as the chemical energy currency. The excitation transport from the absorbing molecular site to the reaction center is mediated by supramolecular structures, which come in different architectures and variable (but always clearly finite, in the sense of being far from the thermodynamic limit) size in different species, with a coexistence of symmetric and disordered structures on different (energy, length-, and time-) scales, e.g., in the photosynthetic antenna protein LHII of purple bacteria, or rather as completely disordered three-dimensional (3D) structures without apparent symmetries, e.g., in the Fenna-Matthews-Olson light-harvesting complex (FMO) of green sulfur bacteria, or in the cryptophyte phycocyanin 645 (PC645) complex of marine algae (85). In general, these supramolecular structures are relatively

ATP: adenosine triphosphate

LHII: photosynthetic antenna protein

FMO: Fenna-Matthews-Olson light-harvesting complex

PC645: phycocyanin 645

QUANTUM THEORY AND PHOTOSYNTHESIS

Ultrafast nonlinear spectroscopy (87) on molecular aggregates such as the FMO complex has revealed signatures of coherent coupling among excitonic states, on transient timescales and at ambient temperatures. This triggered an intense debate on the potential role of nontrivial quantum effects (i.e., quantum phenomena that go beyond defining effective rates that can then be absorbed into effective evolution equations) for the respective biological function. Current candidate scenarios are photosynthesis (79), avian navigation in Earth's magnetic field (88) and olfaction (89), but conclusive evidence for any functional relevance is missing to date.

stiff and exhibit drifts only on timescales much longer than the typical times required for the excitation transport to the reaction center. However, because these are transport phenomena in living organisms, they occur at finite temperature and are certainly subject to some sort of noise, as well as, possibly, to quasi-deterministic (and hitherto very poorly understood) reconformations related to their functional role on larger (time- and length-) scales (see the sidebar Quantum Theory and Photosynthesis) (86).

By now quite firmly consolidated experimental evidence shows that, notwithstanding (or, probably, because of) their intricate architectures and their embedding in a clearly very noisy macrostructure, these supramolecular transport units indeed can sustain coherent superpositions of vibrationally dressed excitonic eigenstates (90),[3] even at ambient temperatures, on transient timescales under laboratory conditions (81, 90–93). What remains, however, a completely open question is whether such quantum superpositions, and the generically associated quantum interference effects, actually do occur in vivo and whether they may be used (whether by nature or by—quantum—engineers) to foster the supramolecular structure's functional purpose.

There are essentially two fundamental reasons why this undeniably highly intriguing question has so far not been answered: On the one hand, given the intrinsic complexity of the object under study, experimentalists have so far been unable to conceive tools of deliberate intervention to enhance or suppress coherences in the supramolecular dynamics, and to unambiguously probe the impact thereof on macroscopic indicators of the transport efficiency, such as, e.g., the quantum efficiency, i.e., the number of charges generated in the reaction center, per incoming photon. Note that such intervention to control radiation transport in complex materials is at least in principle within reach, as has been experimentally demonstrated with photonic nanostructures (94). On the other hand, theory is so far unable to come up with quantitative predictions that are amenable to direct verification by state-of-the-art experiments and distinctive enough to discriminate different transport scenarios. Some approaches, based on very advanced computational physics (or chemistry) with considerable computational overhead, succeed in consistently reproducing experimental data (2, 3, 73), such as to extract effective rates, etc.; however, they neither offer quantitative predictions that could be falsified by experiment nor help us gain a better understanding of the decisive structural elements that guarantee the functional properties of the molecular machines of interest. Another philosophy attempts to grasp these essential structural or dynamical features, often with simple, strongly reductionist quantum dynamical models (69, 71, 72, 95, 96). Although this in principle allows us to define specific and, possibly, mutually exclusive transport scenarios, these models often lack sufficient detail to match realistic experimental

[3]The strength of the coupling between excitonic and vibrational degrees of freedom is, again, widely variable from species to species. The debate on the prevalence of excitonic or vibrational coherence has, however, converged to some sort of consensus that neither one can be completely neglected and that one thus often witnesses vibronic coherences.

conditions, such that experimental data do not allow unambiguous discrimination between them. Hence, what is needed are more refined tools for targeted experimental intervention and more faithful, yet minimalistic, theoretical models that allow integration of the diverse time-, length-, and energy scales that must be orchestrated to achieve and quantify certain functional properties.

Nonetheless, the diverse theoretical approaches currently on the market already account for a good part of the basic ingredients that determine the transport efficiency across the light harvesting unit:

- Coherent transport on short, transient timescales (58, 60, 69, 95–97);
- Dominantly incoherent transport on asymptotic, long timescales (the traditional view in chemical physics) (98);
- Nonnegligible coupling between excitonic and vibrational degrees of freedom (90), or, to some extent equivalently;
- Structured spectral densities of the environmental degrees of freedom coupled to the excitonic manifold (99, 100); and
- statistical variations of transport efficiencies upon sampling over different conformational realizations (58, 96, 97, 101).

Let us now describe an elementary network model that can accommodate these diverse features, inspired by the phenomenology of the FMO unit.

2.1. Transport Efficiencies Across Random Networks

According to currently available structure data, the FMO is a three-dimensional molecular network composed of seven or eight molecular sites defined by the locations of its constituent chlorophyll units (85). In the desire to faithfully represent the FMO's excitonic spectrum (which mediates the excitation transport), the chlorophylls are modeled as dipolar molecules with two electronic (ground and excited) states, which are coupled to each other through dipole-dipole interactions. The relative positions and orientations of the constituent molecular dipoles, the on-site electronic energy levels, and the inter-site coupling strengths are tabulated in the literature (102, 103). Slight variations between different references and the always relatively large error bars that garnish the tabulated numerical values are an expression of the fact that these are, and, given the complexity of the object of interest, ought to be, effective descriptions, which imply strong coarse graining, i.e., an effective average over the many unresolved degrees of freedom of the supramolecular structure. Indeed, these available effective descriptions are deduced by careful deduction of coupling strengths, etc., from experimental data as well as from state-of-the-art structure calculations. In particular, in an interdisciplinary context and discourse it is crucial to fully appreciate this rather fundamental distinction between the experimental and theoretical analysis of quantum dynamics in a physical chemistry or biophysics setting in contrast to the, by their very construction, highly controlled and engineered objects of quantum optical experiments and theory.[4] Furthermore, note that, though the chlorophyll molecules that define the network's sites are a priori identical, the on-site energies of the tabulated effective FMO Hamiltonians are not; i.e., they exhibit some nontrivial potential landscape, which is due to the individual chlorophylls' "local environments" (102, 103). In biophysics jargon, this refers to shifts of the electronic eigenenergies through local couplings to background degrees of freedom that, e.g., span the supramolecular conformation space.

[4]Hamiltonians are engineered as naked as they stand, with excellent control on the errors incurred by neglect of weakly coupled, well-defined degrees of freedom (104).

Hence, quantum transport of a single excitation across the FMO molecular network is generated by an effective N-site Hamiltonian operating on an N-dimensional Hilbert space. At present, consensus is that it is extremely unlikely that more than one excitation at a time is injected into the network, which also eases dynamical simulations considerably (also see Section 3 below).[5]

Given the above, a natural and popular approach to modeling excitation transport on the FMO network is by quantum dynamical simulation, which essentially propagates a suitably chosen initial condition over relevant timescales (107). In general, this is done by numerical solution of some effective evolution equation for the open system quantum dynamics of the FMO Hamiltonian coupled to some environment with possibly structured spectral density (71–73). The structured part of the environment's spectral density accounts for the possibly strong coupling to selected environmental degrees of freedom, which may give rise to non-Markovian memory effects (108) in the open system time evolution (99). An alternative to the description by a non-Markovian environment consists in incorporating the prominent environmental degrees of freedom (which cause the structured component of the spectral density) into the system Hamiltonian [then no more a strictly excitonic Hamiltonian representing one single effective degree of freedom, but "dressed" by a background, e.g., vibrational coordinate, in close analogy to dressed state descriptions of light-matter interaction, e.g., in quantum optics (104) and strong field physics (109)], which then interacts with a Markovian (structure-less) bath (65). Finally, the environment coupling may also incorporate the irreversible dissipation into a sink attached to a specific network site; this accounts for the desired delivery of the excitation to the reaction center (110, 111).

Such a quantum dynamical approach is indeed capable of qualitatively reproducing most experimentally observed features—long-lived coherences among excitonic states, which manifest, e.g., in a damped beating signal of suitably defined correlation functions, non-Markovian effects induced by a structured (vibrational) environment, noise-induced transport across a disordered network with excitonic eigenstates that are localized on a finite subset of the molecular sites, and coherent transport mediated by vibrational dressing of the excitonic manifold. If excitation transport units like the FMO compound have been optimized by evolution, e.g., for rapid and complete excitation transfer, this picture suggests a carefully tuned interplay of coherent, incoherent, and dissipative couplings to delocalize excitonic transport, bridge energy gaps, and induce directionality toward the reaction center. However, this is a conclusion based on the simulated dynamics generated by an averaged, effective Hamiltonian, whereas individual complexes differ in their microscopic structures, giving rise to measurably different (91) dynamical evolutions. One needs to remember then that, in general, the quantum dynamics on disordered systems is not self-averaging, i.e.,

$$\langle e^{-itH} \rangle_{\text{disorder}} \neq e^{-it\langle H \rangle_{\text{disorder}}}, \qquad 1.$$

such that the above optimization argument ultimately hinges on the ambient noise overriding the Hamiltonian structure to induce efficient diffusive, classical transport (112). This is in line with the traditional view that, at ambient temperatures, all transport must ultimately be driven by stochastic activation. Whether classical diffusive transport is compatible with experimentally observed timescales remains a matter of controversial debate in the literature (113–115).

Another approach to revealing the potential of nontrivial quantum effects to enhance the functionality of molecular networks à la FMO is statistical rather than dynamical in spirit. According to the above, the object of interest is the statistical distribution of transport coefficients, as generated by e^{-itH} when sampling over the different physical realizations of H as present in

[5]This observation is also relevant for the discussion on whether coherence effects can play a role in vivo, when the sample is excited by sunlight, i.e., an incoherent source, rather than by coherent laser radiation (105, 106).

the given organism. The underlying intuition stems from the quantum transport theory of finite, disordered systems: Because disorder-induced quantum interference effects as Anderson localization are a consequence of destructive multipath interference upon transmission, characteristic transport coefficients will exhibit strong fluctuations from realization to realization (because each realization defines a different interference condition), for a finite sample length (116). Indeed, in the Anderson case these fluctuations are exponentially large and define an unambiguous hallmark of quantum interference (117). Consequently, in disordered, finite networks there must be finite probability for strongly interference-enhanced transmission probabilities. At least on transient timescales (on which, in a noisy environment, quantum coherence can at best survive), this picture will be qualitatively unaffected by the ambient noise, which, however, will dominate on asymptotic timescales (111).

Although dipole-coupled networks as realized by the molecular aggregates we are here interested in do not give rise to Anderson localization in a strict sense [because this type of inter-site coupling does not induce exponentially localized eigenstates (78)], they still give rise to multipath interference, with relative phases that must sensibly depend on the specific conformation of the network. If we model the network Hamiltonian as

$$H = \sum_{i \neq j=1}^{N} v_{i,j} |j\rangle\langle i|, \qquad 2.$$

where the sum runs over all pairs of distinct N network sites[6] and the inter-site dipole-dipole coupling $v_{i,j}$ is determined by distance and relative dipole orientation, different conformations will lead to different realizations of the Hamiltonian. Such Hamiltonians (Equation 2) generate excitonic dynamics on a fully connected random network, where an excitation is destroyed at site i and created at site j, mediated by the coupling strength $v_{i,j}$. Energy is transferred across the network like a quasiparticle.

In contrast to the above quantum dynamical point of view, which considers the average Hamiltonian structure as the actual structure generating the dynamics, one can now adopt the somewhat complementary point of view and assume that the complex's conformations are randomly distributed, e.g., within a sphere where input (where the photon is absorbed) and output (where the excitation is eventually delivered to the reaction center) sites are fixed at the north and south poles, respectively. Thus, random positioning of the intermediate chlorophyll sites induces a random distribution of the coupling matrix elements in Equation 2, through $v_{i,j} \propto r_{i,j}^{-3}$ [if the relative dipole orientations are neglected, which does not change the qualitative picture (58)], and thus gives rise to conformation-dependent transport coefficients. If the latter are defined by what has been baptized the "transfer efficiency" (69),

$$\mathcal{P}_H = \max_{t \in [0, T_R)} \left| \langle \text{out} | e^{-iHt} | \phi(0) \rangle \right|^2, \ |\phi(0)\rangle = |\text{in}\rangle, \qquad 3.$$

with T_R a suitably defined benchmark time (see below), then $\mathcal{P}_H$ must exhibit strong fluctuations under random changes of the network conformation, according to the above intuition, and this is confirmed by numerical simulations as displayed in **Figure 1**.

What becomes evident from these results is that, whereas the average transfer efficiency over the entire statistical sample of Hamiltonians (Equation 2) is indeed low (~5%), as expected from common sense expectations on the localization properties of excitonic eigenstates on random structures, there does exist a nonnegligible subset of Hamiltonian realizations that give rise to

[6] This includes the input and output sites, $|\text{in}\rangle = |1\rangle$ and $|\text{out}\rangle = |N\rangle$.

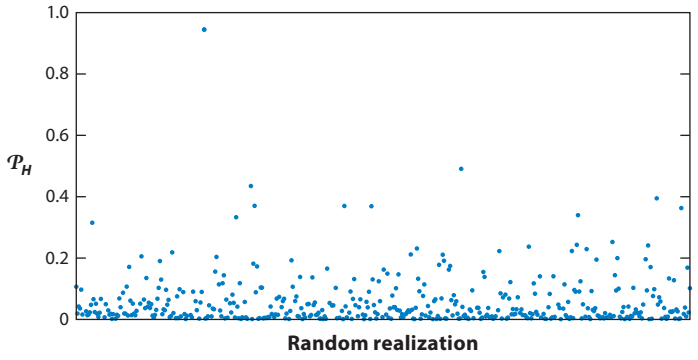

Figure 1

Excitation transfer efficiencies $\mathcal{P}_H$, as defined by Equation 3, across random realizations of an $N = 7$ site random network (69). The latter is described by Equation 2, with $T_R = \pi/20|V|$, $V = v_{\text{in,out}}$, input and output sites located at the north and south pole of a sphere, and the intermediate sites, $N = 2, \ldots, 6$, randomly distributed within the sphere, to randomize the coupling matrix elements $v_{i,j}$ in Equation 2. Although the majority of network realizations gives rise to rather moderate transfer efficiencies $\mathcal{P}_H \simeq 5\%$, there is a finite subset of realizations that generate significantly more efficient transport, up to values not too far from unity. Because the dynamics is purely coherent, this is a result of constructive multipath interference between the different transmission amplitudes connecting input to output.

transfer efficiencies much above average, and in some cases close to unity (somewhere between 50% and 100%). Because, under conditions of strictly unitary transport as here assumed, the transfer efficiency is essentially given by the spectral decomposition of the unitary generated by H,

$$|\langle \text{out}|U(t)|\text{in}\rangle|^2 = |\sum_j \langle \text{out}|\eta_j\rangle\langle\eta_j|\text{in}\rangle \exp(-iE_j t/\hbar)|^2; \quad 4.$$

such high transfer efficiencies imply the existence of at least one excitonic eigenstate $|\eta_j\rangle$ that exhibits an appreciable overlap with both $|\text{in}\rangle$ and $|\text{out}\rangle$.

2.2. Constraints to Optimize Transport Across Disordered Networks

It now immediately comes to mind to optimize a given random Hamiltonian with respect to the transfer efficiency, and, indeed, genetic algorithms (118) seeded with any one of the Hamiltonians that give rise to typical transfer efficiencies in **Figure 1** rapidly converge into strictly optimal Hamiltonians, which quickly depopulate the input site and coherently feed all population into the output site (see **Figure 2**) (58). But which are the specific features that render such Hamiltonians optimal? When inspecting their spatial structure, no apparent symmetries stand out, and in this sense the problem is somewhat reminiscent of the optimal pulse shapes generated by genetic algorithms (119) or other optimization strategies (120) for optimal coherent control: Also there, the generated optimal pulse shapes reveal generally little about which underlying principle defines the optimal superposition of paths in state space to optimize the given target functional. However, the time dependence of the different sites' populations as displayed in **Figure 2** exhibits such sought-for symmetry, with the additional prominent feature that the input and output sites' populations largely dominate over those of the intermediate sites (which, nonetheless, and importantly, remain nonnegligible). A sufficient condition to generate such symmetry on the time axis is the centrosymmetry (121) of the underlying Hamiltonian, i.e., the property that H be symmetric under mirroring with respect to its center, for some labelling of the network sites. More formally speaking, this is tantamount to the commutation relation $JH = HJ$, with the exchange operator

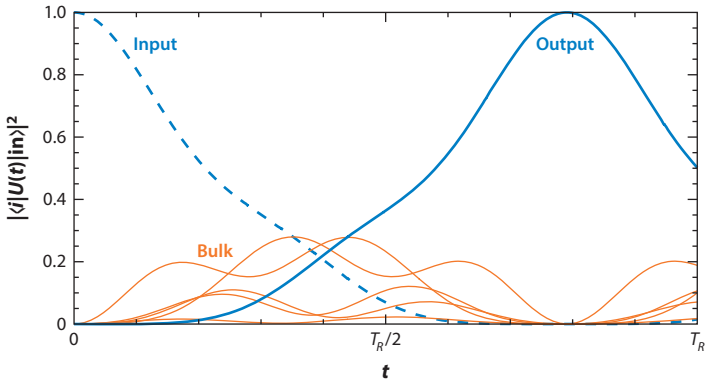

Figure 2

Populations of input, output, and bulk sites, as a function of time (in units of the benchmark time T_R), for an $N = 7$ network optimized by a generic algorithm seeded with a typical low-efficiency configuration as represented by low values of $\mathcal{P}_H$ in **Figure 1** (58). Because the dynamics is purely coherent, the observed time evolution must be quasi-periodic. Strikingly, the populations are indeed periodic, and (approximately) mirror-symmetric with respect to a time $t^*/2$; i.e., $|\langle i \mid \phi(t)\rangle|^2 \simeq |\langle Ji \mid \phi(t^*/2 - t)\rangle|^2$. The time evolution of input and output sites is strongly reminiscent of the dynamics of a wave packet in a double well potential. The mirror symmetry on the time axis is suggestive of a centrosymmetric structure of the underlying Hamiltonian, whereas the effective double well dynamics is indicative of a dominant doublet in the spectral structure, with a weight α (see Equation 6) that is determined by the relative amplitudes of the input and output site populations as compared with that of the bulk states.

$J_{i,j} = \delta_{i,N-j+1}$, together with $|\mathrm{in}\rangle = J|\mathrm{out}\rangle$. A possible measure of centrosymmetry is then given by

$$\epsilon = \frac{1}{N} \min_{\sigma} ||H - J^{-1}HJ||, \qquad 5.$$

where minimization is performed over permutations σ of the intermediate sites $2, \ldots, N-1$, $||.||$ denotes the Hilbert-Schmidt-norm, and small values of ϵ correspond to pronounced centrosymmetry and vice versa. Equation 5 now allows inspection of the correlation between centrosymmetry and transfer efficiency, as shown in **Figure 3**: Indeed, the correlation is unambiguous and shows that centrosymmetry of H is a design principle that is very favorable to improve the transport properties of the network. Yet it is not sufficient, as the distribution of transfer efficiencies for given ϵ still almost covers the entire interval $[0, 1]$.

Here helps the second observation from above: Not only are the populations of the network's sites symmetric on the time axis but also the populations of the input and output sites dominate over the intermediate sites' populations, at almost all times (except $t \simeq t^*/2$; see **Figure 2**). Furthermore, if taken alone, the time evolution of input and output site populations is almost a textbook example of the time evolution of the populations of a double well's right and left sites when initiated, e.g., on the left. Therefore, what we are facing in the case of optimal transport is effective double well dynamics—in chemical jargon, connecting the donor and the acceptor site—with the intermediate sites simply adjusting the tunneling barrier. Consequently, the eigenvectors $|\tilde{\eta_j}\rangle$ of H are expected to exhibit a dominant doublet $|\tilde{\pm}\rangle$ with weight

$$\alpha = |\langle \tilde{\pm}|\pm\rangle|^2 \gg |\langle \tilde{\eta_j}|\pm\rangle|^2 \,, \; \forall \tilde{\eta_j} \neq \tilde{\pm}, \qquad 6.$$

where $|\pm\rangle = (|\mathrm{in}\rangle \pm |\mathrm{out}\rangle)/\sqrt{2}$. Equation 6 defines a "second design principle," beyond the above centrosymmetry.

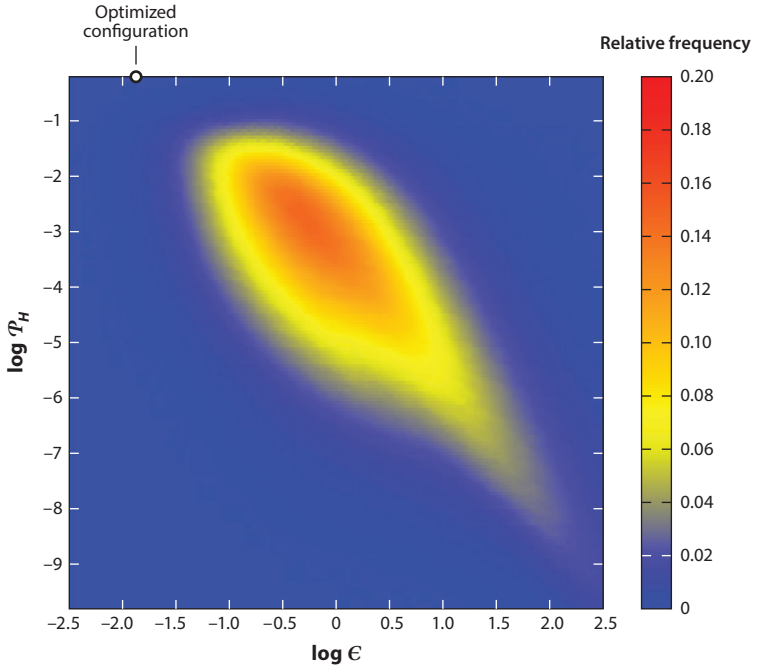

Figure 3

Correlation between the network's centrosymmetry quantified by ϵ, as defined by Equation 5 (the smaller ϵ, the more centrosymmetric the network) and its transfer efficiency $\mathcal{P}_H$, as defined by Equation 3, in a double logarithmic plot. The correlation is unambiguous and confirms that centrosymmetry favors the probability of efficient excitation transfer. Yet centrosymmetry does not allow for a safe bet. An additional design principle is needed. The observed correlation is a consequence of quantum interference upon transmission across the network and fades away under noise (97). The white dot on the top left of the plot represents the optimized network configuration that generates the time evolution displayed in **Figure 2**.

With this intuition gained from the simulation of excitation transport across random networks of the type defined in Equation 2, one can now formulate a transport theory for finite-size random Hamiltonians with a structure constrained by the above design principles (61). To ease a (still rather nontrivial) analytical treatment, we abandon the geometrical construction of random Hamiltonians via randomized relative positions $r_{i,j}$ within a sphere and rather employ $N \times N$ Hamiltonians from the Gaussian orthogonal ensemble (GOE) (122) of random matrix theory (RMT).

For each realization, $|\text{in}\rangle$ and $|\text{out}\rangle$, fulfilling the constraint $|\text{in}\rangle = \boldsymbol{J}|\text{out}\rangle$, are associated with those sites i and $N - i + 1$ that exhibit the weakest direct coupling matrix element $V = \min_i |H_{i,N-i+1}|$. A thus generated random Hamiltonian constrained by centrosymmetry and the presence of a dominant doublet has the general structure

$$H = \begin{pmatrix} E+V & \langle \mathcal{V}^+| & & \\ |\mathcal{V}^+\rangle & H^+_{sub} & & \\ & & E-V & \langle \mathcal{V}^-| \\ & & |\mathcal{V}^-\rangle & H^-_{sub} \end{pmatrix}, \qquad 7.$$

with $\langle \pm | H | \pm \rangle = E \pm V$, and $|\mathcal{V}^\pm\rangle$ random vectors with Gaussian distributed entries, which mediate the coupling between the dominant doublet and the eigenstates of the GOE sub-matrices $H^\pm_{sub}$. The Hamiltonian's specific block-diagonal structure is inherited from its representation in

GOE: Gaussian orthogonal ensemble

RMT: random matrix theory

the centrosymmetry eigenbasis: Because $HJ = JH$, these operators share a joint set of eigenstates, and the degeneracy of J thus induces the block-diagonal structure of H. Phrased differently, the centrosymmetry introduces parity as a quantum number. Note that the upper block of Equation 7, indicated by "+", represents the even parity eigenstates of the network, whereas the block labeled by "−" depicts the odd parity subspace. The representation in the centrosymmetry (or parity) eigenbasis is crucial for these structures to emerge.

Because the dominant doublet weight α needs to be close to unity, by its very definition, the coupling to the random states associated with the randomly coupled intermediate molecular sites is weak and can be accounted for perturbatively. Despite being weakly coupled, the collective effect of the intermediate sites amounts to a shift of the doublet states that, if garnished with the proper sign, can enormously enhance the unperturbed, direct tunnel splitting V, even in the limit of vanishing direct coupling. Because the tunneling time is just the inverse of the effective tunneling splitting, this amounts to a potentially strongly accelerated tunneling process, which possibly allows it to prevail over the timescales of competing loss processes (e.g., recombination of the excitation, which is not incorporated in the above Hamiltonian), and, thus, to achieve what quantum opticians dub strong coupling (104). Note that this scenario is an incidence of what has been conceived as chaos-assisted tunneling (CAT) (123) in the quantum chaos literature: If direct tunneling between the potential wells of a symmetric double well in one degree of freedom is strongly suppressed, the nonlinear coupling to a second degree of freedom may generate "chaotic" eigenstates (124), which sensibly depend on a control parameter and are themselves weakly coupled to the original tunneling doublet. The resulting effective tunneling rate between the wells can then be shown to exhibit strong fluctuations under changes of the control parameter, and may be enhanced by orders of magnitude, through the weak coupling to the chaotic states. In our present example, the random positioning of the intermediate sites, modeled by GOE matrices, mimics the chaoticity induced by the coupling to the additional degree of freedom in the CAT scenario, which is perfectly adequate in view of the, to date, well verified Bohigas-Giannoni-Schmidt conjecture (125). Indeed, as discussed earlier, statistical scatter of the entries of the effective Hamiltonians of FMO-like complexes is due to changes of the local environment as defined by the molecular complexes' conformational structures, which amounts to nothing else but the coupling to other degrees of freedom (e.g., of vibrational character). This statistical scatter is in the present statistical model generated by random sampling over the GOE ensemble.

Given Equation 7, it is possible to generalize the random matrix theory of CAT for our present purposes and to derive the distribution of excitation transfer times and efficiencies, as well as the scaling behavior thereof with the size of the network (either at fixed spectral density or at fixed direct tunneling coupling V) (61). Here we only illustrate the effect of the above design principles on the distribution of transfer efficiencies, in **Figure 4**.

Whereas an unconstrained GOE random network generates a broad distribution of transfer efficiencies with rather unsatisfactory average performance, centrosymmetry shifts this distribution to larger average values, though without much narrowing. The dominant doublet requirement, however, induces a dramatic sharpening of the distribution, which is sharply peaked above $\mathcal{P}_H > 2\alpha - 1$, thus leading to an almost deterministic transport from input to output site, without precise knowledge of the positioning of the intermediate sites. Only coarse grained quantities fix this dynamical behavior: The average level density of the bulk states (essentially controlled by the packing of the molecular sites), the average coupling strength of input and output sites to the bulk, and the dominant doublet strength α. Note that, though it may appear obvious that a doublet structure can guarantee deterministic transport from donor to acceptor, the mechanism described above allows embedding such a structure into a random network of N sites, without appreciable change of the relevant properties of the doublet's eigenvectors while strongly shortening the

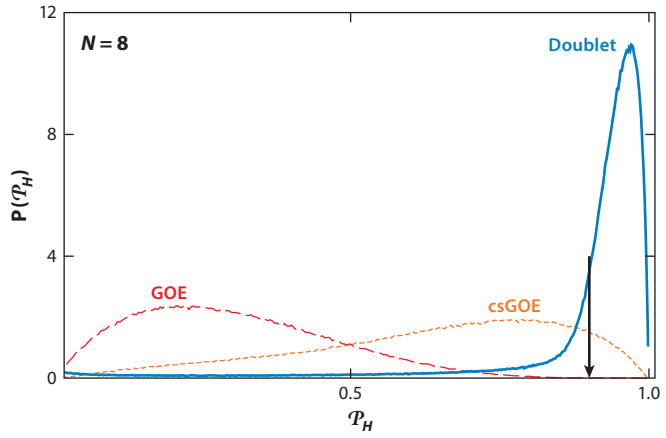

Figure 4

Control of the distribution of transfer efficiencies (with $T_R = \pi/2|V|$) of $N = 8$ site random networks sampled from the Gaussian orthogonal ensemble (GOE) matrices, through additional constraints. Whereas the unconstrained GOE ensemble gives rise to a broad distribution of transfer efficiencies with its center in the vicinity of 20%, the centrosymmetry constraint (as quantified by Equation 5) generates the centrosymmetric GOE (csGOE) ensemble with a still broad distribution of efficiencies, though with a maximum clearly shifted to appreciable values around 80%. When those centrosymmetric networks are post-selected, which on top exhibit a dominant doublet with weight $\alpha = 0.9$ (see Equation 6), the distribution narrows down dramatically and allows for almost deterministic delivery of the excitation at the output site, without control of the microscopic positioning of the bulk sites. Only the average density of states in the bulk, the number of network sites, and the average coupling strength between bulk and input and output sites suffice to fix the distribution. A random matrix theory (RMT) treatment (61, 96) allows prediction of a lower bound for the maximum of the dominant doublet distribution, here marked by an arrow.

transfer times. No detailed knowledge on the microscopic hardwiring of the entire structure is needed, except for the centrosymmetry requirement. In particular, this mechanism allows for a robust implementation of interference-induced enhancement of the transfer efficiency, because only the above-mentioned coarse grained parameters must be under control.

Let us stress that the above CAT-inspired transport optimization scheme strictly relies on constructive multipath quantum interference upon transmission across the network, and it cannot be reproduced by classically diffusive transport. This can be qualitatively verified by adding, e.g., dephasing noise locally at each molecular site. Once the noise is strong enough to induce approximately one incoherent event per coherent transfer time across the sample, the above correlation between centrosymmetry and transfer efficiency fades away, and the coherent tunneling between donor and acceptor starts to be corrupted (97). Owing to its strictly coherent character, CAT optimization furthermore only induces rapid oscillations of the excitation between donor and acceptor, and delivery to the sink—e.g., through connection to a lead—is not incorporated into the model. However, it can be shown that weak coupling to a sink does not qualitatively alter the dynamics but simply turns the system's excitonic eigenstates into resonances with small decay rates, the latter then feeding the reaction center through the sink (58, 111). This is a well-established scenario in mesoscopic physics and light-matter interaction, in which weak coupling to a continuum allows for probing the bound state dynamics without much perturbing it (126). Yet it is currently not well documented how excitations are fed into and extracted from FMO-like molecular networks. One may think of slow, directional leakage (occurring over many near-coherent oscillations between donor and acceptor), which is easy to implement because it only requires weak coupling between,

e.g., the output site and the reaction center, as well as, at least in principle, of precisely timed extraction by molecular reconformation when the excitation arrives at the output site. The latter would require a much higher level of orchestration of excitonic and conformational dynamics than the former, but given the stunningly high degree of specialization of these biological functional units, it may be premature to fully exclude such a scenario.

STED: stimulated emission depletion

2.3. State of Affairs and Directions to Follow

Where do we stand? Beating signals from nonlinear spectroscopy on photosynthetic light-harvesting units gave us new, intriguing reasons to think anew about the interplay of disorder, interference, and noise when it comes to describing and controlling quantum transport on finite size networks embedded in noisy environments. As far as the transport of single excitations is concerned, it is now clear that constrained disorder allows rather impressive and robust control of transport efficiencies on short timescales, whereas noise takes over on long timescales and overwrites the underlying Hamiltonian structures (by mixing the associated eigenstates). If constraints like the ones suggested above are relevant for the observed transfer efficiencies, then characteristic traits thereof must emerge from spectroscopic data even upon averaging over different realizations of the microscopic network structure, and some recent experimental findings could possibly be interpreted in favor of such a hypothesis, because certain transition frequencies are robust against disorder averaging in recent spectroscopic data (92). In addition, statistical spread of coherent transfer timescales has been unambiguously observed in single molecule experiments (91) and, thus, appears to favor the relevance of the distribution of microscopic Hamiltonian structures rather than noise enhanced transport on the averaged structure. However, producing large statistical data sets on biological samples is a truly difficult experimental challenge, and a comparison between theory and experiment is therefore uncertain.[7] Furthermore, given the immense variety of light-harvesting units implemented by nature, it appears at our present state of knowledge inappropriate to discard any currently proposed mechanism, be it classical, i.e., noise-induced, or quantum, i.e., interference-induced.

Still, neither one of these models is so far able to come up with distinctive and experimentally verifiable predictions. On the experimental side, this is due to so far suboptimal control of initial conditions, the lack of tools for selective intervention [such as controlled, locally induced nonlinearities (94) or a controlled admixture of noise (127)], and limitations in resolution [note, however, stimulated emission depletion (STED) (128), even given that its current version requires light intensities that would damage the samples here under study]. Somewhat worse, on the theoretical side, it is clear that purely dynamical approaches are unfit for obtaining a qualitative understanding of the working principles of biological functional units, simply owing to the underlying complexity and the concomitant statistical variation. Statistical and dynamical tools will need to be merged. Furthermore, models such as the ones sketched above must be enlarged to explicitly incorporate those structures that feed the absorbed photon's energy into the molecular network, as well as the connection to and the charge separation within the reaction center. This could define a first model of sufficient complexity to assess, perhaps even quantitatively, one of the decisive, experimentally accessible figures of merit, the quantum efficiency, i.e., the number of charges produced per incoming photon. In addition, such modeling would mimic transport and conversion dynamics on broadly distributed timescales (from femtoseconds to nanoseconds), with quantum effects certainly confined to the shorter ones. Because much of the excitement about

[7] But a comparison may be in reach (R. Cogdell, private communication).

excitation transport in light-harvesting machines stems from the possible functional relevance of nontrivial quantum effects, this is likely to be the ultimate challenge, as one needs to establish that the macroscopically observed quantum efficiency sensibly depends on a quantum coherent feature on microscopic length- and timescales. At our present state of knowledge, quantum speedup of excitation transfer on the scale of molecular transport complexes like FMO, as, e.g., provided by the above CAT mechanism, would on large length- and timescales just define a distribution of effective transfer rates, with the distribution itself being truly quantum [because it is brought about by quantum interference, which is somewhat similar to mesoscopic conductance fluctuations (129) or Ericson fluctuations (130)]. However, it must then be shown that such a specific (quantum) type of distribution hard wires a functional advantage on large scales.

Finally, there are certain more or less tacit assumptions which await clarification. One relevant and actually also fundamentally interesting issue is the difference between photons coming from the Sun as compared with those coming from a laser source in the lab (101, 105, 106, 113, 114, 131). When analyzing the steady state of an FMO-like structure under solar irradiation it is relatively straightforward to see that coherences cannot be sustained. However, it is also clear that, if these molecular complexes process excitations one by one, we are not talking about characterizing a nonequilibrium steady state, but rather about coherences on transient timescales. Whether such transient coherences can be induced by the absorption of a single photon remains to be analyzed in detail (though all the technical tools are available to do so). Another interesting issue, for the understanding but possibly also for control of the debated transport processes, is the role of nonlinearities, due, e.g., to double excitations (132). Can such events, even if rare, affect the transport efficiency, and can deliberately induced double excitations be used as an experimental diagnostic tool?[8]

3. MANY-PARTICLE TRANSPORT ON RANDOM NETWORKS

Above, we inspected quantum transport of a single excitation across a finite, disordered network and analyzed the impact of additional constraints on the statistics of a characteristic transport quantifier. In closing, we also remarked that one of the open questions to be addressed is the influence of nonlinearities on the transport properties. One possibility for creating nonlinearities is by feeding more than one excitation or particle into the network. Indeed, the quantum dynamics of interacting many-particle systems, on regular or disordered lattices, is a long-standing, multifaceted, and highly nontrivial research area (135–138). It recently enjoys some renewed interest, not least owing to the availability of experimentally controlled many-particle systems of diverse natures (139–145). Depending on the system's size and on the physical nature of its constituents, different theoretical toolboxes are employed and blended in the different communities' jargon. However, in substance, the relevant unsolved questions remain:

- How do many-particle interactions or nonlinearities affect quantum transport phenomena (49) on regular as well as on disordered lattices?[9]
- How do statistically robust, macroscopic observables emerge from the microscopic description of many-particle quantum systems of increasing complexity, in equilibrium and out of equilibrium? What is, eventually, the specific role of interactions/nonlinearities (48, 52)?

[8]Compare, e.g., Coulomb and Rydberg blockade effects in mesoscopics (133) and quantum optics (134).

[9]Note that, on the level of the fundamental equations, nonlinearities in interacting cold matter systems have many similarities to well-known phenomena in nonlinear optics, and that nonlinearities affect (actually in a similar, maybe universal manner) quantum transport in a priori very distinct physical settings, from light-matter interaction over condensed, possibly soft matter and mesoscopic physics to quantum simulations!

- What is the potential of controlled nonlinearities as a means to control quantum transport (94), in particular in complex structures?

Rather than follow this line of thought, which arguably merits an independent review, we here take one step back and acknowledge another feature that automatically comes into play when injecting more than one particle, which is fundamentally quantum in its very nature—rather than the perfectly classical notion of interactions—and prevails also in the absence of the latter: the indistinguishability of identical particles. Even in the absence of particle-particle interaction the indistinguishability multiplies the alternatives that mediate transport from input to output of some device or network. Consequently, the amplitudes associated with these alternatives must be summed up coherently to infer the probability of a certain transmission event. In other words, now Young's double slit is no more the only elementary building block, as in the previous section, because not only do single-particle amplitudes interfere with each other, but so do many-particle amplitudes. This generates some rather unexpected effects, even in the absence of interactions, for relatively small particle numbers and on small, regular networks (37, 38, 43, 146–148). Furthermore, the number of interfering alternatives grows rapidly with the particle number and, thus, defines an interesting incident of indistinguishability-induced "complexity" (148, 149).

3.1. Mapping Many-Particle Input on Many-Particle Output States

Let us consider our transport problem under a slightly different perspective now, in second quantized form. The network can be described by a unitary matrix U that maps input channels i on output channels o, via

$$a_i^\dagger \to \sum_o U_{i,o} b_o^\dagger, \qquad 8.$$

where the physical nature of the indistinguishable particles (fermions or bosons) is implied through the (anti-)commutation relations of the creation and annihilation operators $a_i^\dagger$, $b_o^\dagger$ and a_i, b_o, respectively. The symmetries and/or irregularities of the network are determined by the complex-valued entries of U. If we prepare an input state $|\text{in}\rangle$ by distributing N particles over $M \geq N$ input channels, such that at most one particle is injected into a channel (this allows for a direct comparison of fermionic and bosonic transport), i.e.,

$$|\text{in}\rangle = a_{i_1}^\dagger \ldots a_{i_N}^\dagger |\Omega\rangle\,,\ i_j \neq i_k \forall j \neq k, \qquad 9.$$

with $|\Omega\rangle$ being the M-channel vacuum state, then, by virtue of Equation 8, the M-channel output state reads as

$$|\text{out}\rangle = \mathcal{U}|\text{in}\rangle = \sum_{o_1 \ldots o_N = 1}^{M} U_{i_1,o_1} b_{o_1}^\dagger \ldots U_{i_N,o_N} b_{o_N}^\dagger |\Omega\rangle. \qquad 10.$$

This also defines $\mathcal{U}$, the unitary operator on Fock space, which implements the map (Equation 8).

For the minimal scenario where $M = N = 2$ and U represents a balanced beam splitter,

$$a_1^\dagger \to (b_1^\dagger + b_2^\dagger)/\sqrt{2},\ a_2^\dagger \to (b_1^\dagger - b_2^\dagger)/\sqrt{2}, \qquad 11.$$

with one photon (thus, bosonic commutation rules) injected into each of the input modes, this induces the following mapping from input to output state:

$$|1,1\rangle = a_1^\dagger a_2^\dagger |\Omega\rangle \to \frac{1}{2}\left[(b_1^\dagger)^2 - b_1^\dagger b_2^\dagger + b_2^\dagger b_1^\dagger - (b_2^\dagger)^2\right] = \frac{1}{2}\left[(b_1^\dagger)^2 - (b_2^\dagger)^2\right] = \frac{1}{2}(|2,0\rangle - |0,2\rangle), \qquad 12.$$

with vanishing probability for the coincident output event $|\text{out}\rangle = |1,1\rangle$, where one photon is detected in each output mode. This is a consequence of the destructive interference of the two

MANY-PARTICLE INTERFERENCE WITH/OUT DISTINCTIVE DEGREES OF FREEDOM

Additional degrees of freedom can be added by structuring the single-particle Hilbert space $\mathcal{H} = \mathcal{H}_{\text{modes}} \otimes \mathcal{H}_{\text{internal}}$, where $\mathcal{H}_{\text{modes}}$ represents the mode structure of the main text and $\mathcal{H}_{\text{internal}}$ represents all additional degrees of freedom. To correctly populate Fock space, one defines new, nonorthogonal, creation and annihilation operators: $[a_i(\phi), a_j^\dagger(\psi)] = \langle \phi \mid \psi \rangle \delta_{ij}$, where $|\phi\rangle, |\psi\rangle \in \mathcal{H}_{\text{internal}}$, and i and j label the modes. Because these additional degrees of freedom are assumed to be untouched by the propagation through the network, applying this to the HOM setup results in

$$a_1^\dagger(\phi) \to \left[b_1^\dagger(\phi) + b_2^\dagger(\phi) \right] / \sqrt{2}\,, \; a_2^\dagger(\psi) \to \left[b_1^\dagger(\psi) - b_2^\dagger(\psi) \right] / \sqrt{2}. \tag{13.}$$

When performing a measurement, one typically does not consider the internal degrees of freedom, and, therefore, the probability $P_{1,1}$ to measure the particles in different modes is given by

$$P_{1,1} = \frac{1}{4} \sum_{k,l} \left| \langle \Omega | b_1(\eta_k) b_2(\eta_l) \left[b_1^\dagger(\phi) + b_2^\dagger(\phi) \right] \left[b_1^\dagger(\psi) - b_2^\dagger(\psi) \right] | \Omega \rangle \right|^2 = \frac{1}{2} \left(1 - |\langle \phi \mid \psi \rangle|^2 \right), \tag{14.}$$

where $\{\eta_i\}$ form a basis of $\mathcal{H}_{\text{internal}}$. The result for distinguishable particles is recovered whenever $|\langle \phi \mid \psi \rangle|^2 = 0$. By contrast, when the particles cannot be distinguished by this internal degree of freedom, we obtain the result for pure, indistinguishable bosons.

two-particle transmission amplitudes $a_1^\dagger a_2^\dagger \to b_1^\dagger b_2^\dagger$ and $a_1^\dagger a_2^\dagger \to b_2^\dagger b_1^\dagger$ in Equation 12, known as the Hong-Ou-Mandel (HOM) (or Shih-Alley) effect (150, 151), and is the second fundamental building block that complements Young's double slit when considering many-particle transport.

Note that the prediction of Equation 12 differs dramatically from the prediction for distinguishable (classical) particles, in which the coincident output event would occur with a probability of 1/2. Also note that, despite this completely different probability distribution for two-particle output events, the single-mode particle density expectation values $\langle b_o^\dagger b_o \rangle$ are identical (unity) for classical particles or bosons. This highlights the fact that many-particle interference effects cannot be witnessed on the level of single-channel observables but require a correlation measurement (such as the measurement of the coincident event's probability) between distinct output ports (147).[10] Consequently, we expect that, for a general unitary U and arbitrary $M \geq N$, quantum transport across the sample represented by U will exhibit dramatic signatures of the particles' indistinguishability, in multichannel correlation functions measured on output. Mutatis mutandis, as the particles lose their indistinguishability, e.g., by adding an additional degree of freedom that allows for the distinction of sub-groups of particles (in the language of decoherence theory, this is tantamount to providing Welcher Weg information, now in the space of many-particle trajectories), these signatures of many-particle interferences must fade away. This has indeed been demonstrated experimentally, though with the further subtlety that many-particle interference signals do in general exhibit a nonmonotonous distinguishability transition if the latter is controlled by a single continuous parameter (38) (see the sidebar Many-Particle Interference With/Out Distinctive Degrees of Freedom).

HOM: Hong-Ou-Mandel or Shih-Alley effect

[10] Nowadays, HOM has become a diagnostic tool in photonics when the indistinguishability of photons needs to be certified. The vanishing of the coincident event probability is a sensitive—interference-based—test of the precision of the two-photon state's preparation.

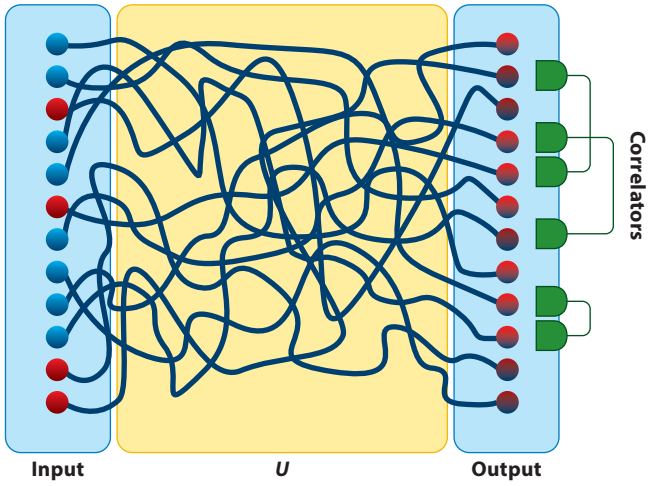

Figure 5

Many-particle transport scenario across a random network represented by a unitary random matrix U sampled over the Haar measure. Particles of variable quantum statistical nature—distinguishable, fermionic, bosonic—are prepared in the input state $|\text{in}\rangle$, defined by Equation 9, and injected at the red input sites, with no more than one particle per site (to allow for a direct comparison of fermionic and bosonic transport properties). Because the computational overhead may grow exponentially with the number of particles and the size of the system, an exhaustive characterization of the many-particle output state is in general prohibitive. For a statistical characterization, two-point correlation functions (Equation 18) among all pairs of distinct output sites are sampled, to build the C-data set, which then can be characterized by its lower statistical moments (Equation 19).

3.2. Many-Particle Transport Across Large, Disordered Networks

This brings us back to our overarching theme of disordered networks. When injecting an indistinguishable many-particle state as defined in Equation 9 into a disordered network described by a unitary U (see **Figure 5**), we expect strong signatures of many-particle interference on output, according to our above considerations. At first glance, this is reminiscent of the interference-induced transmission fluctuations, which we described in the previous Section 2, because the larger the network, the larger the number of interfering transmission amplitudes. In the present multi-particle case, however, a severe additional problem kicks in: Not only does the number of transmission amplitudes proliferate but now the dimension of the space of output states also increases exponentially with the particle number. Indeed, the computational effort to evaluate the transition probability between some many-particle input state $|\text{in}\rangle$ and another many-particle output state $|\text{out}\rangle$ amounts to evaluating the following:

- The permanent of a real matrix, for distinguishable particles;
- the determinant of a complex matrix, for fermions; and
- the permanent of a complex matrix, for bosons.

Although efficient algorithms (in the sense of algorithmic complexity theory) are able to efficiently simulate distinguishable particles and fermions, simulation of the bosonic case is considered to be computationally hard (149) (see the sidebar Boson Sampling).

In other words, the exhaustive quantitative characterization of $|\text{out}\rangle$ very quickly exhausts any computational device, as well as a dedicated experimentalist, and thus renders a statistical treatment

BOSON SAMPLING

Complexity is a widely used term that is attributed somewhat different—community-dependent—flavors. In the natural sciences, complexity is associated with chaos, disorder, pattern formation, and the (computational or experimental) overhead to fully characterize a complex system's state. In computer sciences, it is the complexity of algorithms that is assessed. Though rather distinct fields, the physics of complex systems and computational complexity theory recently met in the boson sampling problem: It is shown that sampling from the output probability distribution, as generated via complex transport (scattering) of noninteracting bosons through a random medium, is computationally hard; i.e., a full characterization of the output state requires an experimental overhead that increases exponentially with the system size. Consequently, the efficient simulation of many-boson interference implies a collapse of the polynomial hierarchy to the third level (149), which challenges many well-established aspects of algorithmic complexity theory. In turn, under the perspective of many-particle transport theory, boson sampling sheds light on rather fundamental aspects of the quantum statistical implications for many-particle dynamics.

imperative, much as in the case of classical thermodynamics: We must identify statistically robust signatures of the many-particle transport, which can be read off from experimental observables with a measurement overhead that scales in a benign way with the size of the problem. Note that this also defines a somewhat paradigmatic incident of quantum simulation and of the associated certification problem (152–158): A photonic circuit that implements U and prepares $|\mathrm{in}\rangle$ can produce output states that cannot be generated computationally, and, in this sense, simulates a problem out of reach for computers. However, for the same reason, it is virtually impossible to certify that the device constructed by the experimentalist does indeed implement U and operates on $|\mathrm{in}\rangle$, at least if the only way of certification consisted in the—experimental or computational—verification of the complete output state.

Depending on the unitary U to be implemented, and on the input state $|\mathrm{in}\rangle$ to be prepared, the certification problem can have different concretizations. If U exhibits some symmetries, these in general (also see our earlier considerations in this review) must manifest themselves in suitably chosen transport quantifiers. Furthermore, to fully characterize the sample, a single input state in general does not suffice, owing to the weights $\langle\mathcal{E}_j|\mathrm{in}\rangle$ (see Equation 4), where $|\mathcal{E}_j\rangle$ are the eigenvectors of $\mathcal{U}$, which (implicitly) enter Equation 10. Thereby, only that part of the spectrum of $\mathcal{U}$ is probed that has been selected by the local density of states $|\langle\mathcal{E}_j|\mathrm{in}\rangle|^2$.[11] Consequently, one needs to seek certification on the basis of quantities that are obtained by taking averages over the realization of U (and hence of $\mathcal{U}$) and/or over $|\mathrm{in}\rangle$. In the following, we elaborate on the case of random U taken from the Haar measure (see the sidebar Haar Measure), such as to mimic a completely unstructured random network, and input states as specified by Equation 9.

We seek to certify the specific dynamical signature of the injected particles' quantum statistics by characteristic interference structures in the many-body transmission signal. As we saw above at the elementary example of the HOM setup, the quantum statistical nature already has a strong impact on the level of two-point correlation functions. We assume that M and N are significantly

[11] Only if a "generic" input state, i.e., a state sufficiently different from an eigenstate of $\mathcal{U}$ and not too close to the edge of the spectrum, has an essentially flat local density of states will a single input state suffice (under a suitable average). This condition is largely equivalent to requiring that U be generated by a random Hamiltonian chosen from a random matrix ensemble or that an underlying classical phase space exhibit strictly hyperbolic structure. More recently, this property is being rediscussed under the keyword "eigenstate thermalization" (159).

HAAR MEASURE

Probability measures occur in many forms and with many structures; some are more natural than others. Perhaps the most natural of all is the uniform distribution that appoints the same weight to all elements in the set under consideration. A type of set that is often treated in measure theory and has particular relevance in physics is compact topological groups. It can be shown (160) that, for any compact topological group $\mathcal{G}$, there exists a unique measure μ, called the Haar measure, with the following properties:

$$\begin{aligned} \mu(\mathcal{G}) &= 1, \\ \mu(\mathcal{O}) &> 0 \text{ for every nonempty open set } \mathcal{O} \subset \mathcal{G}, \\ \mu(g\mathcal{M}) &= \mu(\mathcal{M}g) = \mu(\mathcal{M}) \text{ for all } g \in \mathcal{G} \text{ and every measurable set } \mathcal{M} \subset \mathcal{G}. \end{aligned}$$

As a result of the last property, this measure can be interpreted as the uniform distribution on such groups. In quantum transport theory and quantum chaos, one often considers the group of all $N \times N$ unitary matrices, $\mathcal{U}(N)$, on which a Haar measure can be constructed. In RMT, the set of unitary matrices equipped with its Haar measure is also referred to as the circular unitary ensemble (122).

larger than two in our present case and build a statistical data set from two-point correlation functions evaluated on $|\text{out}\rangle$. Beyond the intuition gained from HOM, another reason why this can be expected to bear a clear signature of the interfering particles' nature (with the interfering amplitudes defined by the specific choice of U) is the different order number of interfering many-particle amplitudes for different particle species, as expressed by the abovementioned, distinct mathematical structures of the transition probabilities from $|\text{in}\rangle$ to $|\text{out}\rangle$: The number of interference terms is largest in the bosonic case, and this should, in a sense to be quantified, produce the "most structured" transmission signal. Our statistical quantity to sample is thus chosen to be the truncated two-point correlation function

$$C_{i,j} = \langle n_i n_j \rangle - \langle n_i \rangle \langle n_j \rangle \,, \; i \neq j \in [1; M] \,, \; n_i = b_i^\dagger b_i, \tag{15.}$$

to provide us with the C-data set. Given M, N, and a realization of U, Equation 18 as well as its lower statistical moments can be evaluated analytically to finally obtain closed expressions (slightly bulky, but trivially evaluable rational functions of N and M) for the normalized mean NM, the coefficient of variation CV, and the skewness S of the C-data set, defined as

$$\begin{aligned} \text{NM} &= \frac{\mathbb{E}_U(C) M^2}{N}, \\ \text{CV} &= \frac{\sqrt{\mathbb{E}_U(C^2) - \mathbb{E}_U(C)^2}}{\mathbb{E}_U(C)}, \\ \text{S} &= \frac{\mathbb{E}_U(C^3) - 3\mathbb{E}_U(C)\mathbb{E}_U(C^2) + 2\mathbb{E}_U(C)^3}{\left[\mathbb{E}_U(C^2) - \mathbb{E}_U(C)^2\right]^{3/2}}, \end{aligned} \tag{16.}$$

where $\mathbb{E}_U$ is the average over the unitary group under the Haar measure. **Figure 6** clearly demonstrates, for $N = 6$ and $M = 13$, respectively, that the different particle species are statistically perfectly well discernable and that the RMT prediction derived from Equation 19 perfectly fits the numerically generated data.

We thus have succeeded in devising a set of statistical, easily computable and measurable quantifiers that unambiguously certify the transmitted particle species—through the characteristic features of many-particle interference signals generated by random unitaries (152). When the

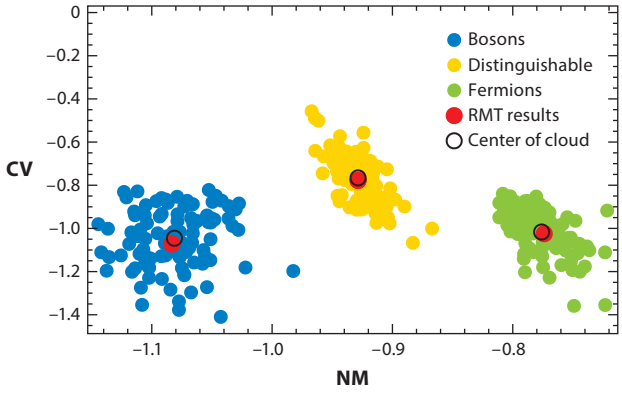

Figure 6

Statistical certification of the transmitted particles' specific scattering dynamics, as determined by the scattering matrix U and the particles' quantum statistical nature. Quantifiers are the normalized mean, NM, and the coefficient of variation, CV, of the C-data set generated by sampling the correlation function $C_{i,j}$ (see Equation 18), over all output ports $i \neq j$ of the network (see **Figure 5**), for $N = 3$ particles fed into an array of $M = 13$ input ports. The colored scattered data points result from direct numerical simulation for one single random unitary and variations of the input ports populated by the N-particle input state (Equation 9). Mean values thereof are indicated by the open circles, which coincide with the analytical random matrix theory (RMT) prediction (152) (given by rather bulky rational expressions in N and M). This latter agreement implies yet another confirmation of the Bohigas-Giannoni-Schmidt conjecture.

underlying dynamics exhibits additional structure or symmetries, we expect certification to be eased (158), and thus we have here sketched out how to deal with some sort of worst case scenario. Blending structural and disorder features will be the next natural step to further refining our understanding of the dynamical consequences of indistinguishability.

SUMMARY POINTS

1. Quantum transport on finite disordered networks is dominated by strong, interference-induced fluctuations.
2. The statistics of characteristic transport coefficients can be controlled by imposing coarse grained constraints while maintaining disorder on the microscopic level. By construction, this defines a robust, statistical control strategy for transport on disordered networks.
3. The dynamics of multiple excitations on a network gives rise to characteristic many-body interference effects (to be distinguished from simple bunching or anti-bunching!), indicative of the quantum statistical nature of the interfering particles, on the level of multi-point correlation functions on output.
4. A statistical analysis of the characteristic interference structures imprinted on low-order correlation functions evaluated on the many-particle output state allows the unambiguous distinction between fermionic, bosonic, and distinguishable particle dynamics, with moderate experimental and computational overhead.

FUTURE ISSUES

1. Embedding finite disordered networks into superstructures as characteristic, e.g., of the photosynthetic apparatus of algae and plants or also of organic PV devices, will allow assessment of the potential advantage of quantum transport on microscopic scales for the overall functionality.
2. Experimental tools must be developed that allow us to select and possibly knock-out specific coherent transition amplitudes.
3. Observables must be defined that distinguish bunching effects from bona fide bosonic many-particle interference contributions.
4. Partial distinguishability (161, 162) of the particles can be accounted for by introducing an additional continuous degree of freedom which may convey Welcher Weg information on the level of many-particle transition amplitudes. This will allow incorporation of unavoidable experimental imperfections for boson sampling certification schemes, but also opens novel perspectives for the decoherence theory of many-particle quantum systems.

DISCLOSURE STATEMENT

The authors are not aware of any affiliations, memberships, funding, or financial holdings that might be perceived as affecting the objectivity of this review.

ACKNOWLEDGMENTS

A.B. thanks Uzy Smilansky and Rami Band and colleagues for one week of discussions on random graphs, back in 2009 in Freiburg, which somewhat seeded our interest in this direction. We are grateful to Torsten Scholak, Tobias Zech, Jonathan Brugger, Roberto Mulet, Spiros Skourtis, Rodolfo Jalabert, Greg Scholes, Rienk van Grondelle, Tjaart Krueger, Richard Cogdell, Bruno Robert, Tönu Pullerits, Harald Kauffmann, Dominique Delande, Shaul Mukamel, Graham Fleming, and Birgitta Whaley for many, and often nicely engaged, controversial debates on the possible role of quantum effects for biological functionality. Furthermore, we would like to give credit to Klaus Mayer, Malte C. Tichy, Juan-Diego Urbina, Jack Kuipers, and Klaus Richter for the fruitful cooperation on boson sampling and related issues. M.W. and F.S. acknowledge financial support from the German National Academic Foundation.

LITERATURE CITED

1. Imry Y. 2009. *Introduction to Mesoscopic Physics*. Oxford, UK: Oxford Univ. Press
2. May V, Kühn O. 2011. *Charge and Energy Transfer Dynamics in Molecular Systems*. Weinheim, Ger.: Wiley-VCH, 3rd ed.
3. Nitzan A. 2006. *Chemical Dynamics in Condensed Phases: Relaxation, Transfer and Reactions in Condensed Molecular Systems. Oxford Graduate Texts*. Oxford, UK/New York: Oxford Univ. Press
4. d'Arcy MB, Godun RM, Summy GS, Guarneri I, Wimberger S, et al. 2004. *Phys. Rev. E* 69:027201
5. Wimberger S, Guarneri I, Fishman S. 2004. *Phys. Rev. Lett.* 92:084102
6. Johnson TH, Clark SR, Jaksch D. 2014. *EPJ Quantum Technol.* 1:1–12
7. Schneider C, Porras D, Schaetz T. 2012. *Rep. Prog. Phys.* 75:024401

8. Feynman R, Leighton R, Sands M. 2013. *The Feynman Lectures on Physics*, Vol. III, *Quantum Mechanics*. Pasadena, CA: Calif. Inst. Technol.
9. Englert BG. 2013. *Eur. Phys. J. D* 67:1–16
10. Albada MPV, Lagendijk A. 1985. *Phys. Rev. Lett.* 55:2692–95
11. Anderson PW. 1958. *Phys. Rev.* 109:1492–505
12. Casati G, Guarneri I, Shepelyansky D. 1988. *IEEE J. Quantum Electr.* 24:1420–44
13. Mishchenko MI. 1993. *Ap. J.* 411:351–61
14. Moore FL, Robinson JC, Bharucha C, Williams PE, Raizen MG. 1994. *Phys. Rev. Lett.* 73:2974–77
15. Schelle A, Delande D, Buchleitner A. 2009. *Phys. Rev. Lett.* 102:183001
16. Ringot J, Szriftgiser P, Garreau JC, Delande D. 2000. *Phys. Rev. Lett.* 85:2741–44
17. Chabé J, Lemarié G, Grémaud B, Delande D, Szriftgiser P, Garreau JC. 2008. *Phys. Rev. Lett.* 101:255702
18. Bayfield JE, Casati G, Guarneri I, Sokol DW. 1989. *Phys. Rev. Lett.* 63:364–67
19. Sirko L, Bauch S, Hlushchuk Y, Koch PM, Blümel R, et al. 2000. *Phys. Lett. A* 266:331–35
20. Galvez EJ, Sauer BE, Moorman L, Koch PM, Richards D. 1988. *Phys. Rev. Lett.* 61:2011–14
21. Jörder F, Zimmermann K, Rodriguez A, Buchleitner A. 2014. *Phys. Rev. Lett.* 113:063004
22. Krug A, Buchleitner A. 2005. *Phys. Rev. A* 72:061402
23. Maeda H, Gallagher TF. 2004. *Phys. Rev. Lett.* 93:193002
24. Abrahams E, Anderson PW, Licciardello DC, Ramakrishnan TV. 1979. *Phys. Rev. Lett.* 42:673–76
25. Hu H, Strybulevych A, Page JH, Skipetrov SE, van Tiggelen BA. 2008. *Nat. Phys.* 4:945–48
26. Sperling T, Bührer W, Aegerter CM, Maret G. 2013. *Nat. Photon.* 7:48–52
27. Wegner F. 1979. *Z. Phys. B* 35:207–10
28. Roati G, D'Errico C, Fallani L, Fattori M, Fort C, et al. 2008. *Nature* 453:895–98
29. Fyodorov YV, Ossipov A, Rodriguez A. 2009. *J. Stat. Mech.* 2009:L12001
30. Rodriguez A, Vasquez LJ, Slevin K, Römer RA. 2010. *Phys. Rev. Lett.* 105:046403
31. Vollhardt D, Wölfle P. 1980. *Phys. Rev. B* 22:4666–79
32. Billy J, Josse V, Zuo Z, Bernard A, Hambrecht B, et al. 2008. *Nature* 453:891–94
33. Wolf PE, Maret G. 1985. *Phys. Rev. Lett.* 55:2696–99
34. Bergmann G. 1984. *Phys. Rep.* 107:1–58
35. Kuga Y, Ishimaru A. 1984. *J. Opt. Soc. Am. A* 1:831–35
36. Peruzzo A, Lobino M, Matthews JCF, Matsuda N, Politi A, et al. 2010. *Science* 329:1500–3
37. Tichy MC, Lim HT, Ra YS, Mintert F, Kim YH, Buchleitner A. 2011. *Phys. Rev. A* 83:062111
38. Ra YS, Tichy MC, Lim HT, Kwon O, Mintert F, et al. 2013. *PNAS* 110:1227–31
39. Meinert F, Mark M, Kirilov E, Lauber K, Weinmann P, et al. 2014. *Phys. Rev. Lett.* 112:193003
40. Murmann S, Bergschneider A, Klinkhamer V, Zürn G, Lompe T, Jochim S. 2015. *Phys. Rev. Lett.* 114:080402
41. Labeyrie G, de Tomasi F, Bernard JC, Müller C, Miniatura C, Kaiser R. 1999. *Phys. Rev. Lett.* 83:5266
42. Modugno G. 2010. *Rep. Prog. Phys.* 73:102401
43. Tichy MC, Tiersch M, de Melo F, Mintert F, Buchleitner A. 2010. *Phys. Rev. Lett.* 104:220405
44. Shapiro B. 2012. *J. Phys. A: Math. Theor.* 45:143001
45. Mosk A, Lagendijk A, Lerosey G, Fink M. 2012. *Nat. Photon.* 6:283
46. Ahlbrecht A, Alberti A, Meschede D, Scholz V, Werner A, Werner R. 2012. *New J. Phys.* 14:073050
47. Kolovsky AR, Buchleitner A. 2003. *Phys. Rev. E* 68:056213
48. Ponomarev AV, Madroñero J, Kolovsky AR, Buchleitner A. 2006. *Phys. Rev. Lett.* 96:050404
49. Geiger T, Wellens T, Buchleitner A. 2012. *Phys. Rev. Lett.* 109:030601
50. Spethmann N, Kindermann F, John S, Weber C, Meschede D, Widera A. 2012. *Phys. Rev. Lett.* 109:235301
51. Nelson J. 2003. *The Physics of Solar Cells*. London/River Edge, NJ: Imp. Coll. Press
52. M.-J. Giannoni, A. Voros JZJ, ed. 1991. *Chaos and Quantum Physics. Les Houches Summer School of Theoretical Physics.* Amsterdam: North-Holland
53. Arndt M, Hornberger K. 2014. *Nat. Phys.* 10:271–77
54. Kottos T, Smilansky U. 1999. *Ann. Phys.* 274:76–124
55. Smilansky U. 2007. *J. Phys. A: Math. Theor.* 40:F621
56. Mülken O, Blumen A. 2011. *Phys. Rep.* 502:37–87

57. Venegas-Andraca SE. 2012. *Quantum Inf. Process.* 11:1015–106
58. Scholak T, de Melo F, Wellens T, Mintert F, Buchleitner A. 2011. *Phys. Rev. E* 83:021912
59. Hul O, Ławniczak M, Bauch S, Sawicki A, Kuś M, Sirko S. 2012. *Phys. Rev. Lett.* 109:040402
60. Mostarda S, Levi F, Prada-Gracia D, Mintert F, Rao F. 2013. *Nat. Commun.* 4:2296
61. Walschaers M, Mulet R, Wellens T, Buchleitner A. 2015. *Phys. Rev. E* 91:042137
62. Barra F, Gaspard P. 2001. *Phys. Rev. E* 65:016205
63. Fyodorov YV, Savin DV. 2012. *Phys. Rev. Lett.* 108:184101
64. Gaspard P. 2014. *Scholarpedia* 9:9806
65. Breuer HP, Petruccione F. 2002. *The Theory of Open Quantum Systems*. Oxford, UK/New York: Oxford Univ. Press
66. Tichy MC. 2014. *J. Phys. B: At. Mol. Opt. Phys.* 47:103001
67. Mandel O, Greiner M, Widera A, Rom T, Hänsch TW, Bloch I. 2003. *Phys. Rev. Lett.* 91:010407
68. Jaksch D, Zoller P. 2005. *Ann. Phys.* 315:52–79
69. Scholak T, Mintert F, Wellens T, Buchleitner A. 2010. *Semicond. Semimet.* 83:1–38
70. Rodriguez A, Chakrabarti A, Römer RA. 2012. *Phys. Rev. B* 86:085119
71. Plenio MB, Huelga SF. 2008. *New J. Phys.* 10:113019
72. Mohseni M, Rebentrost P, Lloyd S, Aspuru-Guzik A. 2008. *J. Chem. Phys.* 129:174106
73. Ishizaki A, Fleming GR. 2009. *PNAS* 106:17255–60
74. Johnson MW, Amin MHS, Gildert S, Lanting T, Hamze F, et al. 2011. *Nature* 473:194–98
75. Crespi A, Osellame R, Ramponi R, Brod DJ, Galvão EF, et al. 2013. *Nat. Photon.* 7:545–49
76. Metcalf BJ, Thomas-Peter N, Spring JB, Kundys D, Broome MA, et al. 2013. *Nat. Commun.* 4:1356
77. Günter G, Schempp H, Robert-de-Saint-Vincent M, Gavryusev V, Helmrich S, et al. 2013. *Science* 342:954–56
78. Scholak T, Wellens T, Buchleitner A. 2014. *Phys. Rev. A* 90:063415
79. Scholes GD, Mirkovic T, Turner DB, Fassioli F, Buchleitner A. 2012. *Energy Environ. Sci.* 5:9374–93
80. Ishizaki A, Fleming GR. 2012. *Annu. Rev. Condens. Matter Phys.* 3:333–61
81. Falke SM, Rozzi CA, Brida D, Maiuri M, Amato M, et al. 2014. *Science* 344:1001–5
82. Tamura H, Burghardt I. 2013. *J. Am. Chem. Soc.* 135:16364–67
83. Amerongen Hv, Valkunas L, Grondelle Rv. 2000. *Photosynthetic Excitons*. Singapore: World Sci.
84. Bardeen CJ. 2014. *Annu. Rev. Phys. Chem.* 65:127–48
85. Blankenship RE. 2002. *Molecular Mechanisms of Photosynthesis*. Oxford, UK/Malden, MA: Blackwell Sci.
86. Krüger TPJ, Wientjes E, Croce R, Grondelle Rv. 2011. *PNAS* 108:13516–21
87. Mukamel S. 2009. *Principles of Nonlinear Optical Spectroscopy. No. 6 in Oxford Series in Optical and Imaging Sciences.* New York: Oxford Univ. Press
88. Winklhofer M, Dylda E, Thalau P, Wiltschko W, Wiltschko R. 2013. *Proc. R. Soc. B* 280:20130853
89. Franco M, Turin L, Mershin A, Skoulakis EMC. 2011. *PNAS* 108:3797
90. Christensson N, Kauffmann HF, Pullerits T, Mancal T. 2012. *J. Phys. Chem. B* 116:7449–54
91. Hildner R, Brinks D, Nieder JB, Cogdell RJ, van Hulst NF. 2013. *Science* 340:1448–51
92. Romero E, Augulis R, Novoderezhkin VI, Ferretti M, Thieme J, et al. 2014. *Nat. Phys.* 10:676–82
93. Engel GS, Calhoun TR, Read EL, Ahn TK, Mancal T, et al. 2007. *Nature* 446:782–86
94. Muskens OL, Venn P, van der Beek T, Wellens T. 2012. *Phys. Rev. Lett.* 108:223906
95. Alicki R, Miklaszewski W. 2012. *J. Chem. Phys.* 136:134103
96. Walschaers M, Fernandez-de-Cossio Diaz J, Mulet R, Buchleitner A. 2013. *Phys. Rev. Lett.* 111:180601
97. Zech T, Mulet R, Wellens T, Buchleitner A. 2014. *New J. Phys.* 16:055002
98. Yang M, Fleming GR. 2002. *Chem. Phys.* 275:355–72
99. Nalbach P, Eckel J, Thorwart M. 2010. *New J. Phys.* 12:065043
100. Olbrich C, Strümpfer J, Schulten K, Kleinekathöfer U. 2011. *J. Phys. Chem. B* 115:758–64
101. Manzano D. 2013. *PLOS ONE* 8:e57041
102. Adolphs J, Müh F, Madjet MEA, Renger T. 2007. *Photosynth. Res.* 95:197–209
103. Moix J, Wu J, Huo P, Coker D, Cao J. 2011. *J. Phys. Chem. Lett.* 2:3045–52
104. de Melo F, Buchleitner A. 2010. In *Quantum Information, Computation and Cryptography*, ed. F Benatti, M Fannes, R Floreanini, D Petritis, *Lecture Notes in Physics*, 808:253–76. Berlin/Heidelberg: Springer
105. Brumer P, Shapiro M. 2012. *PNAS* 109:19575–78

106. Chenu A, Brańczyk A, Scholes G, Sipe J. 2015. *Phys. Rev. Lett.* 114:213601
107. Sarovar M, Ishizaki A, Fleming GR, Whaley KB. 2010. *Nat. Phys.* 6:462–67
108. Lambropoulos P, Nikolopoulos GM, Nielsen TR, Bay S. 2000. *Rep. Prog. Phys.* 63:455
109. Faisal F. 1987. *Theory of Multiphoton Processes*. Berlin/Heidelberg, Ger.: Springer
110. Mülken O, Blumen A, Amthor T, Giese C, Reetz-Lamour M, Weidemüller M. 2007. *Phys. Rev. Lett.* 99:090601
111. Scholak T, Wellens T, Buchleitner A. 2011. *J. Phys. B: At. Mol. Opt. Phys.* 44:184012
112. Scholak T, Wellens T, Buchleitner A. 2011. *Europhys. Lett.* 96:10001
113. Kassal I, Yuen-Zhou J, Rahimi-Keshari S. 2013. *J. Phys. Chem. Lett.* 4:362–67
114. Jesenko S, Žnidarič M. 2013. *J. Chem. Phys.* 138:174103
115. Wilkins DM, Dattani NS. 2015. *J. Chem. Theory Comput.* 11(7):3411–19
116. Kramer B, MacKinnon A. 1993. *Rep. Prog. Phys.* 56:1469
117. Pichard JL, Zanon N, Imry Y, Douglas Stone A. 1990. *J. Phys.* 51:587–609
118. Hansen N. 2006. In *Towards a New Evolutionary Computation*, ed. JA Lozano, P Larrañaga, I Inza, E Bengoetxea, *Studies in Fuzziness and Soft Computing*, 192:75–102. Berlin/Heidelberg Ger.: Springer
119. Pearson BJ, White JL, Weinacht TC, Bucksbaum PH. 2001. *Phys. Rev. A* 63:063412
120. Khaneja N, Reiss T, Kehlet C, Schulte-Herbrüggen T, Glaser SJ. 2005. *J. Magn. Reson.* 172:296–305
121. Cantoni A, Butler P. 1976. *Linear Algebra Appl.* 13:275–88
122. Akemann G, Baik J, Di Francesco P, eds. 2011. *The Oxford Handbook of Random Matrix Theory*. Oxford, UK/New York: Oxford Univ. Press
123. Tomsovic S, Ullmo D. 1994. *Phys. Rev. E* 50:145–62
124. Stöckmann HJ. 2006. *Quantum Chaos: An Introduction*. Cambridge, UK: Cambridge Univ. Press, paperback version, (with corr.) ed.
125. Bohigas O, Giannoni MJ, Schmit C. 1984. *Phys. Rev. Lett.* 52:1–4
126. Buchleitner A, Delande D, Zakrzewski J, Mantegna RN, Arndt M, Walther H. 1995. *Phys. Rev. Lett.* 75:3818–21
127. Blümel R, Buchleitner A, Graham R, Sirko L, Smilansky U, Walther H. 1991. *Phys. Rev. A* 44:4521
128. Hell SW, Wichmann J. 1994. *Opt. Lett.* 19:780–82
129. Jalabert RA, Baranger HU, Stone AD. 1990. *Phys. Rev. Lett.* 65:2442–45
130. Ericson T. 1960. *Phys. Rev. Lett.* 5:430–31
131. Mančal T, Valkunas L. 2010. *New J. Phys.* 12:065044
132. Abramavicius D, Voronine DV, Mukamel S. 2008. *PNAS* 105:8525–30
133. Beenakker CWJ. 1991. *Phys. Rev. B* 44:1646–56
134. Urban E, Johnson TA, Henage T, Isenhower L, Yavuz DD, et al. 2009. *Nat. Phys.* 5:110–14
135. Bardeen J, Cooper LN, Schrieffer JR. 1957. *Phys. Rev.* 108:1175–204
136. Gross EP. 1961. *Nuovo Cim.* 20:454–77
137. Dalfovo F, Giorgini S, Pitaevskii LP, Stringari S. 1999. *Rev. Mod. Phys.* 71:463–512
138. Verbeure AF. 2011. *Many-Body Boson Systems: Half a Century Later. Theoretical and mathematical physics*. London/New York: Springer
139. Will S, Best T, Braun S, Schneider U, Bloch I. 2011. *Phys. Rev. Lett.* 106:115305
140. Hänsel W, Hommelhoff P, Hänsch TW, Reichel J. 2001. *Nature* 413:498–501
141. Genske M, Alt W, Steffen A, Werner AH, Werner RF, et al. 2013. *Phys. Rev. Lett.* 110:190601
142. Kielpinski D, Monroe C, Wineland DJ. 2002. *Nature* 417:709–11
143. Petta JR, Johnson AC, Taylor JM, Laird EA, Yacoby A, et al. 2005. *Science* 309:2180–84
144. Sansoni L, Sciarrino F, Vallone G, Mataloni P, Crespi A, et al. 2012. *Phys. Rev. Lett.* 108:010502
145. Wenz AN, Zürn G, Murmann S, Brouzos I, Lompe T, Jochim S. 2013. *Science* 342:457–60
146. Lim YL, Beige A. 2005. *New J. Phys.* 7:155
147. Mayer K, Tichy MC, Mintert F, Konrad T, Buchleitner A. 2011. *Phys. Rev. A* 83:062307
148. Tichy MC, Tiersch M, Mintert F, Buchleitner A. 2012. *New J. Phys.* 14:093015
149. Aaronson S, Arkhipov A. 2013a. *Theory Comput.* 9:143–252
150. Shih YH, Alley CO. 1988. *Phys. Rev. Lett.* 61:2921–24
151. Hong CK, Ou ZY, Mandel L. 1987. *Phys. Rev. Lett.* 59:2044–46

152. Walschaers M, Kuipers J, Urbina J-D, Mayer K, Tichy MC, et al. 2014. arXiv:1410.8547
153. Bentivegna M, Spagnolo N, Vitelli C, Brod DJ, Crespi A, et al. 2014. *Int. J. Quantum Inform.* 12:1560028
154. Gogolin C, Kliesch M, Aolita L, Eisert J. 2013. arXiv:1306.3995
155. Aaronson S, Arkhipov A. 2014. *Quantum Inf. Comput.* 14(15–16):1383–423
156. Carolan J, Meinecke JDA, Shadbolt PJ, Russell NJ, Ismail N, et al. 2014. *Nat. Photon.* 8:621–26
157. Aolita L, Gogolin C, Kliesch M, Eisert J. 2015. *Nat. Commun.* 6:8498
158. Tichy MC, Mayer K, Buchleitner A, Mølmer K. 2014. *Phys. Rev. Lett.* 113:020502
159. Nandkishore R, Huse DA. 2015. *Annu. Rev. Condens. Matter Phys.* 6:15–38
160. Conway JB. 1997. *A Course in Functional Analysis*. Vol. 96, *Graduate Texts in Mathematics*. New York: Springer, 2nd ed.
161. Shchesnovich VS. 2015. *Phys. Rev. A* 91:013844
162. Tichy MC. 2015. *Phys. Rev. A* 91:022316